Research Square

Preprints are preliminary reports that have not undergone peer review.
They should not be considered conclusive, used to inform clinical practice,
or referenced by the media as validated information.

Microcomb-driven parallel coherent detection and communication enabled by a power-free optical phased array

Yaocheng Shi

yaocheng@zju.edu.cn

State Key Laboratory of Extreme Photonics and Instrumentation,Zhejiang University
https://orcid.org/0000-0003-4489-8310

Shi Zhao

Zhejiang University

Jingyu Zhao

State Key Laboratory of Extreme Photonics and Instrumentation,Zhejiang University
https://orcid.org/0009-0003-8790-671X

Wenke Jiao

State Key Laboratory of Extreme Photonics and Instrumentation,Zhejiang University

Jingye Chen

Zhejiang University

Daixin Lian

State Key Laboratory of Extreme Photonics and Instrumentation,Zhejiang University

Yaongqi Ye

State Key Laboratory of Extreme Photonics and Instrumentation,Zhejiang University

Zhe Kang

Nanjing University of Aeronautics and Astronautics https://orcid.org/0000-0003-4342-026X

Jijun He

Nanjing University of Aeronautics and Astronautics https://orcid.org/0000-0001-7011-4386

Dongmei Huang

Photonics Research Institute, Department of Electrical and Electronic Engineering, The Hong Kong Polytechnic University

Daoxin Dai

Zhejiang University https://orcid.org/0000-0002-2769-3009

Article

Keywords:

Posted Date: August 27th, 2026

DOI: https://doi.org/10.21203/rs.3.rs-10564923/v1

License: This work is licensed under a Creative Commons Attribution 4.0 International License.
Read Full License

Additional Declarations: There is **NO** Competing Interest.

Abstract

The growing demand for high-frame-rate detection and high-capacity communication is accelerating the transition of information carriers from microwaves to optical waves. With its inherent parallelism across multiple wavelengths, the optical frequency microcomb overcomes the high cost and poor scalability bottlenecks associated with discrete lasers, offering a compelling integrated source for emerging applications such as autonomous vehicles and 6G networks. Nevertheless, multi-beam parallel integrated detection and communication (IDC) remains an unmet goal. Moreover, existing parallel detection systems rely on bulk and inertial components for multi-beam manipulation, which undermines the intrinsic potential of microcomb for high-density integration. In this paper, we propose and experimentally demonstrate all-solid-state parallel coherent detection, parallel communication, and parallel IDC systems using silicon nitride based zero power consumption optical phased array (OPA) and microcomb. Through combined waveguide and grating dispersion, the OPA chip directs each comb tooth of the single soliton microcomb to distinct angles without electric-control, thereby generating a zero power consumed two-dimensional beam array. The OPA chip features a mirror-symmetric configuration that doubles the number of resolvable points within a compact chip footprint of 1.8×4.0 mm^2. Using the proposed OPA chips as the transmitter and receiver, parallel coherent detection is demonstrated utilizing frequency-modulated continuous-wave (FMCW) method. Subsequently, we demonstrate parallel free-space optical communication (FSOC) by employing multiple receiving units to independently collect different beams carrying information. Finally, by synergistically integrating the aforementioned light detection and ranging (LiDAR) and FSOC systems, we further demonstrate parallel IDC, where the multiple receiving units simultaneously serve as both targets and users. These results pave the way for realizing all-solid-state, ultra-compact, high-frame-rate coherent LiDAR system, as well as high-capacity, multi-user FSOC system.

1. Introduction

Advancements in intelligent equipment, including robots and autonomous vehicles, rely on efficient and high-precision environmental perception as the foundation for autonomous decision-making and operational safety[1]. As critical nodes in dynamic networks, unmanned systems further demand reliable and high-speed communication links to support real-time transmission and interaction of massive data[2]. Integrated with artificial intelligence, these capabilities collectively drive the evolution toward the Internet of Things (IoTs) and broader intelligentization[3]. Within this framework, high-precision detection serves as the system's "eyes", while wireless communication functions as its "nervous system", both playing indispensable for next-generation intelligent systems.

Leveraging high directionality, coherence, short wavelength, and large bandwidth, the laser serves as an ideal carrier for high-resolution detection[4] and high-capacity wireless communication[5]. However, systems based on a single laser source face inherent limitations: in detection, point-by-point scanning restricts the frame rate due to beam steering and signal processing overhead; in multi-user

communication, time-division multiplexing reduces per-user capacity and increases latency. While deploying multiple discrete lasers provides a straightforward workaround, it incurs a substantial higher cost and system complexity[6,7]. The optical frequency microcombs[8–11] featuring broad spectral span, compact footprint, high coherence, and parallel multi-wavelength output, offers a transformative light source for photonic systems including high-capacity communications[12,13], parallel computing[14,15], and high-efficiency detection[16,17]. A prerequisite for parallel light detection and ranging (LiDAR), parallel free-space optical communication (FSOC), and parallel integrated detection and communication (IDC) is the ability to project individual comb teeth into free space with sufficient angular separation for resolvable detection and reception. To date, however, microcomb based multi-beam parallel FSOC and IDC have not yet been demonstrated. Moreover, reported parallel detection schemes rely on bulk optical assemblies: collimators, transmission gratings and inertial components for beam emission, separation, and steering[16–20]. Such mechanically constrained architectures inherently fall short of exploiting the integration potential of microcombs.

On-chip integrated optical phased arrays (OPA), fabricated using mature semiconductor processes, offer compelling advantages in form factor, cost and stability[21–23], positioning them as a cornerstone technology for next-generation all-solid-state LiDAR and FSOC systems[24,25]. The integrating of OPAs with microcomb presents a promising pathway toward fully solid-state, parallelized architectures[26,27]. Conventional two-dimensional (2D) OPAs rely on an $N \times N$ array of phase shifters to independently control the phase of each radiating antenna element, thereby synthesizing a tilted wavefront for dynamic far-field beam steering[28]. However, this configuration demands N^2 independent control channels, which introduces critical bottlenecks, including a large chip footprint, intricate control schemes, and most notably prohibitively high-power consumption. Furthermore, the inherently limited antenna aperture of 2D OPAs precludes the spatial resolution required to resolve individual microcomb spectral lines, thereby restricting their utility in parallel-operation scenarios. An alternative strategy circumvents these limitations by achieving 2D beam steering with only $N + 1$ control channels through the synergistic combination of a tunable light source and a one-dimensional (1D) OPA[29,30]. In this configuration, the phased array governs beam deflection in one dimension, while wavelength tuning exploits grating diffraction to enable scanning in the orthogonal direction. The 1D OPA architecture relaxes the constraints on antenna aperture length, facilitating substantial reductions in beam divergence—a prerequisite for the spatial separation of microcomb teeth. Nevertheless, realization millimeter-scale grating antennas requires extremely small feature sizes[31] or multi-layer materials[32] to minimize perturbation strength, inevitably escalating fabrication complexity and cost owing to the reliance on high-precision lithography and multilayer thin-film deposition. Moreover, while the 1D OPA reduces the requisite number of phase shifters, it does not fundamentally resolve the persistent challenges of control complexity and excessive power consumption that plague its 2D counterpart.

In this work, we propose and experimentally demonstrate an all-solid-state parallel beams generator that synergistically integrates a microcomb with a co-designed zero power consumption OPA. Unlike conventional OPA architectures, our chip could project each comb tooth to a distinct 2D spatial location

without mechanical parts, ultra-long antennas, or complex phase-shifter control, thereby fundamentally simplifying the system architecture for parallel operation. The proposed OPA leverages a waveguide array featuring a predetermined length gradient, entirely obviating the requirement for active phase shifters. The antenna pitch and delay line differences are jointly optimized to match the frequency spacing of the microcomb, enabling the generating uniformly distributed 2D parallel beams in the far field. The fabricated chip, incorporating a folded mirror configuration, occupies a compact footprint of 1.8×4.0 mm^2. By tuning the light source wavelength from 1510 to 1640 nm at 0.4 nm steps, a field of view of 22.3°×9.1° with approximately 652 addressable spots is achieved. The measured beam divergence is 0.32°×0.15°, with a sidelobe suppression ratio (SLSR) of 10.4 dB. Leveraging the zero power consumption OPA chip to radiate each linearly chirped tooth of the microcomb into 2D space, we conceptually demonstrate a parallel transceiving LiDAR system driven by only a single fixed pump laser, eliminating the requirement for wavelength swept source or active beam-steering elements. Importantly, each parallel comb tooth could also be modulated individually, offering additional flexibility for data encoding. As a proof of concept, we realize parallel FSOC by using the proposed OPA chip to radiate modulated beams into free space with multiple users independently collecting distinct beams carrying high-speed non-return-to-zero (NRZ) signals. Finally, capitalizing on the inherent compatibility of LiDAR and FSOC functionalities, we further demonstrate parallel IDC, wherein the receiving units simultaneously serve as both detection targets and communication users—highlighting the system's potential for unified sensing and data-link operations in future intelligent optical platforms.

Figure 1 presents the schematic of the proposed parallel all-solid-state FMCW LiDAR and FSOC system. The zero power consumption OPAs are utilized as transceiver, which consist of power splitter trees, waveguide delay lines and grating antenna arrays. To enhance the number of resolvable spatial spots, two mirrored OPAs are monolithically integrated on a single chip. The input optical signal is equally divided into 64 channels via a six-stage multimode interference (MMI) power splitter tree. The optimized 1×2 MMI features a width of 6.5 μm, length of 23.8 μm, port distance of 3.4 μm and port width of 2.5 μm. Between the power splitter tree and the antenna array, the waveguide delay line lengths for each channel form an arithmetic progression with an incremental difference ΔL between adjacent channels, as shown in Fig. 1. In the horizontal dimension, the beam angle (θ_x) is dictated by the wavelength-dependent phase gradient established across the antenna array through the waveguide delay lines; in the vertical dimension, θ_y is governed by the grating dispersion (Supplementary Note 1). The delay increment ΔL and the adjacent antennas pitch (P) are chosen as 78.8 μm and 4 μm, respectively, to ensure spectral-spatial matching between the OPA and the microcomb, yielding comparable beam step sizes in both dimensions for parallel detection or communication demonstration. This all-passive design eliminates the requirement for active phase shifters, thereby achieving truly zero static power consumption. To mitigate random phase errors[33] (Supplementary Fig. S1), the waveguide width is adopted as 2 μm. The grating antenna employs a sidewall-etched geometry to simplify the fabrication, with grating width W_{grt}=1.50 μm, period Λ = 1.18 μm, and sidewall etch depth D = 0.25 μm. Critically, the minimum feature size of the OPA chip is 0.25 μm, rendering the device fabrication friendly and compatible with standard CMOS processes.

2. Results

2.1 Beam steering operated by zero power consumption OPA

An optical photograph of the fabricated 2×64 OPA chip placed on a fingertip is shown in Fig. 2(a), illustrating its compact form factor with a total footprint of 1.8×4.0 mm^2. The chip area is substantially reduced by omitting on-chip electrical circuitry. A magnified view highlighting the structural details is provided in Fig. 2(b). We characterize the 2D beam steering ability by recording the far-field intensity distribution with a charge-coupled device (CCD) camera, as shown in Supplementary Note 2 and Fig. S2a. By sweeping the laser wavelength from 1510 to 1640 nm at 0.4 nm steps, the far-field distributions of all beams are obtained, and the superimposed results are shown in Figs. 2(c) and 2(d). Owing to the mirror-symmetric arrangement of OPA1 and OPA2, the far-field beam patterns are symmetric about the antenna's transmission axis, which eliminates blind spots and doubles the number of resolvable far-field spots. The measured field of view is 22.3°×9.1°, corresponding wavelength tuning efficiencies of 1.39°/nm and 0.07°/nm for two axes, respectively. The beam divergence is measured to be 0.32°×0.15° and SLSR is 10.4 dB, as shown in Supplementary Figs. S2b and S2c.

2.2 Parallel FMCW detection and parallel free space communication

LiDAR constructs 3D point clouds of the surrounding environment by measuring target distances across multiple angles. A single soliton microcomb provides a multi-wavelength, parallel, coherent, and continuous-wave source. In this work, the parallel distinguishable beams are generated by integrating the proposed OPA with a single soliton microcomb (Supplementary Note 4). The measured microcomb spectrum and corresponding far-field pattern are shown in Supplementary Fig. S5. To demonstrate parallel coherent detection, we construct a prototype system using two OPA chips as the transmitter (Tx) and receiver (Rx), combining the FMCW method, as illustrated in Fig. 3(a). Details of the experimental setup are provided in the Methods. All comb teeth are modulated simultaneously, with frequency modulation nonlinearity below 6×10^{-6} (Supplementary Note 3 and Note 5). As a proof of concept, we select the 35 comb teeth spanning wavelength from 1534.70 nm to 1565.52 nm for parallel FMCW detection (gray-shaded region in Supplementary Fig. S6b). The frequency spacing between adjacent comb teeth (101.3 GHz) is significantly larger than the beat frequency (< 2.2 GHz) and far exceeds the bandwidth of the BPD (75 MHz). Therefore, the beat signals generated by individual comb teeth can be considered mutually independent and free from interference in the frequency domain interference. For convenient demonstration of parallel FMCW detection, a tunable narrow BPF is placed after the SSB to sequentially select the individual comb teeth. We position a U-shape target with a rectangle board as background in front of the OPA chip. Figure 3(b) presents the measured 3D point clouds alongside a photograph of the targets. The corresponding beat signals spectra are shown in Supplementary Fig. S7, with all signal-to-noise ratios (SNR) exceeding 18 dB. Figure 3(c) summarizes the measured distances

from all detections. The U-shape target and rectangle background are clearly distinguishable, with distances to transceiver of 0.52 m and 0.84 m respectively.

Furthermore, we demonstrate parallel FSOC utilizing the microcomb in conjunction with the proposed OPA, as shown in Fig. 4. Details of FSOC system are described in the Methods. Each parallel comb tooth could be independently modulated, after which the data streams are radiated into free space via the OPA. This configuration enables the delivery of either identical or distinct information to multiple receiving users. As a proof of concept, eleven comb teeth within the gray-shaded region of Supplementary Fig. S8a are selected. The communication links are established at a distance of 1.2 m. The measured SNRs of the eye diagrams for 24 Gbps NRZ on-off-keying (OOK) signals range from 5.9 dB to 6.7 dB, as shown in Fig. 4(b). The SNR variation is attributed to the combined effects of the uneven comb teeth intensity, collimator alignment error, and the wavelength-dependent gain variation of the EDFA. Figure 4(c) presents the measured eye diagram for the comb tooth at 1547.04 nm. The eye diagrams for all comb teeth are provided in Supplementary Fig. S8b. At a wavelength of 1560 nm, the measured SNR of the reference signal at the MZM output port is 9.2 dB (Supplementary Fig. S8b). Compared to the reference signal, the degradation in communication signal is primarily attributed to the noise introduced by EDFA. The measured eye diagrams for each comb tooth remain clear and open, confirming the system's capability for parallel high-speed data transmission.

2.3 Parallel integrated detection and communication

To demonstrate parallel IDC, we employed collimators serving as users, as illustrated in the Fig. 5(a). The subsystem below the dashed line replicates the detection system from Fig. 3(a), while the portion above reproduces the FSOC system from Fig. 4(a). The output of the microcomb is split into two paths, feeding the detection and communication links, respectively. A circulator is introduced at the input of the OPA chip #1 to enable interference-free integration of the two subsystems. The data streams carried by the comb teeth are radiated into free space via the OPA chip #1 after passing through the circulator. Meanwhile, the FMCW detection signals transmitted by the OPA chip #2 (serving as the transmitter) are reflected by the target, and the echo signals received by the OPA chip #1 (serving as receiver) are routed through the circulator to a mixer, where they beat with the local oscillator for detection. The users also serve as detection targets during the communication link establishment process. Figure 5(b) presents the measured beat signal spectra when the comb teeth illuminate the four users, corresponding to wavelength of 1547.04 nm, 1552.04 nm, 1552.88 nm, and 1560.44 nm, respectively. Distinct signal peaks are observed at 1.29 MHz, 1.23 MHz, 1.33 MHz, and 1.37 MHz, corresponding to target distances of 0.73 m, 0.53 m, 0.86 m, and 0.99 m from the OPA chips. For free space communication, the 24 Gbps NRZ OOK data streams, carried by the comb teeth with same wavelengths used for detection, are directed toward the users by OPA chip #1. The measured eye diagrams are shown in Fig. 5(c), with SNRs of 6.1 dB, 5.4 dB, 4.9 dB, and 5.1 dB, respectively.

3. Discussion

In summary, we have proposed and demonstrated a co-designed, zero power consumption OPA chip integrated with an optical frequency microcomb. The fabricated 2×64 passive OPA chip, leveraging both waveguide and grating dispersion, eliminates the need for power-hungry phase shifters and occupies an compact footprint of 1.8×4.0 mm². By employing a mirror-symmetric configuration, the OPA chip doubles the number of resolvable far filed points. The measured field of view and beam divergence are 22.3°×9.1° and 0.32°×0.15° respectively, with a SLSR of 10.4 dB achieved without any power consumption for phase tuning or calibration. Combining the proposed OPA chip with an optical frequency microcomb, we have demonstrated parallel FMCW LiDAR, parallel FSOC, and parallel IDC, validating its potential application in the fields of parallel detection and broadcast parallel wireless communication. With the single soliton microcomb serving as the light source, 2D beam steering is realized without real-time wavelength tuning, effectively reducing the number of control channels to zero. Notably, both the OPA chip and microcomb chip are fabricated on the SiN platform, offering a natural pathway toward monolithic integration. Furthermore, the proposed OPA radiates the comb teeth into free space to generate distinguishable beams array without requiring precisely fabricated grating antennas or phase shifters, significantly reducing the fabrication complexity and simplifying the overall parallel system architecture.

Fully integrated systems represent the prevailing trend in current development and the continuing pursuit for researchers[22,34–38]. The scheme proposed in this work establishes a foundation for enhancing the integration level and reducing overall power consumption of parallel LiDAR and FSOC systems. However, further improvements in the light source and coherent detection modules are essential. On-chip lasers, such as self-injection locked lasers and external cavity lasers, can replace commercial light sources to generate combs via precise frequency and phase tuning[39–41]. Moreover, applying a chirp signal to the integrated laser could eliminate the need for the SSB and RF source[42–45], thereby simplifying the system architecture. Far-field beam power is a critical parameter influencing the LiDAR detection range and FSOC capacity. One effective strategy is to incorporate erbium-doped waveguide amplifier or semiconductor optical amplifier into the OPA chip[46,47], replacing off-chip EDFA and boosting the on-chip guided optical power. Another strategy to enhance the beam power is loss minimization. Monolithically integrating a microcomb with OPA could eliminate coupling loss, while tailored waveguide designs could reshape the far-field profile to concentrate a greater proportion of power into the main lobe, thereby reducing beamforming losses. For parallel coherent detection, a straightforward approach involves the on-chip integration of wavelength division demultiplexer, routing waveguide arrays, and crossing waveguide arrays. This configuration demultiplexes the local oscillator and echo signal according to comb lines prior to detection by a BPD array. An alternative scheme employs two synchronously frequency-modulated microcombs serving as the light source and local oscillator, respectively. This approach distributes the beat frequencies of different channels across the frequency domain, enabling the use of a single coherent detector and greatly simplifying the detection design[18,20]. As discussed, monolithic integration of the microcomb, OPA, optical amplifier, mixer, and other key components on a SiN platform, along with co-integration of laser and detector on the same chip, could enhance system stability, eliminate inter-chip coupling losses, and facilitate wafer-scale manufacturing. We believe that

the approach presented in this work could offer a viable route toward achieving miniaturized, parallel, and low-cost all-solid-state integrated LiDAR system and FSOC system.

4. Methods

Fabrication of microcomb chip and OPA chip

The SiN microring resonators for microcomb generation were fabricated via the standard AN800 multi-project wafer (MPW) run (Ligentec, Switzerland). The proposed OPA chip was fabricated on a 300 nm-thick SiN platform with a 3 μm-thick buried oxide layer. The fabrication process requires only a single lithography step and inductively coupled plasma reactive ion etching (ICP-RIE) process, followed by the deposition of a 2 μm-thick silica cladding via plasma enhanced chemical vapor deposition (PECVD) for protection. Owing to its passive nature, the design eliminates the need for cumbersome overlay alignment and metal deposition steps, substantially reducing manufacturing complexity and cost.

Experimental details

The far-field performance of the fabricated OPA were characterized using a tunable laser (Agilent 81640A) and a charge-coupled device (CCD) camera (Hamamatsu C14041-10U).

The microcomb was generated using a SiN microring resonator (MRR) with radius of 229 μm, corresponding to a free spectral range of 101.3 GHz. The CW pump seed light (Toptica Photonics CTL 1550) was amplified to 200 mW by EDFA. A bandpass filter (WL Photonics WLTF-WM-P-1550-100) was employed to remove amplified spontaneous emission (ASE). The filtered pump light was then coupled into the coupling waveguide of the SiN MRR via a lensed fiber. The pump wavelength was swept from the blue-detuned side to the effective red-detuned side of the cavity resonance. The output spectra of microcomb were measured by an optical spectrum analyzer (Yokogawa AQ6370D).

The linear frequency chirp was generated via external modulation method consisting an arbitrary function generator (SIGLENT SDG6012X-E), a custom-built voltage controlled oscillator (VCO) and a single-sideband modulator system (Fujitsu FTM7962EP and PlugTech MBC-IQ-02). The chirp frequency ranged from 11.2 GHz to 13.4 GHz, corresponding to a bandwidth of 2.2 GHz and a repetition rate of 10 KHz. The chirped optical signal was amplified to 20 mW by an EDFA and then split into two parts with splitting ratio of 99: 1, serving as the signal and local oscillator, respectively. The signal beam was emitted to free space by the Tx OPA. After reflection from the targets, the echo was received by the Rx OPA and mixed with the local oscillator. The combined optical signal was detected by a balanced photodetector (KY-BPRM-75M-I-FA), and the resulting beat frequency was recorded on an oscilloscope (Keysight DSO7032B).

A 24 Gbps NRZ OOK data stream was generated using a programmable pulse generator (Stelight mBT5210) and a commercial lithium niobate Mach-Zehnder modulator (Optilab IMP1550-40-PM). Then, the modulated and amplified data stream was radiated into free space via the Rx OPA and directed

toward a collimator (Thorlabs F810APC-1550). The received signal was amplified, filtered by a bandpass filter (WL Photonics WLTF-WM-P-1550-100) to suppress ASE noise from the EDFA, and then collected by a digital sampling oscilloscope (Keysight DCA-X86100D) for analysis.

Declarations

Competing interests

The authors declare no competing interests.

Author contributions

All authors contributed extensively to the work presented in this paper. Y. S. conceived the study. S. Z., J. Z., J. C., D. D., and Y. S. designed and characterized the OPA chip. Z. K., J. H., and D. H. designed and characterized the comb chip. S. Z., J. Z., W. J., D. L., and Y. Y. performed the system measurements. All authors participated in data analysis and discussion. S. Z., J. Z., J. C., Z. K., D. D., and Y. S. conducted theoretical analysis. S. Z., J. Z., J. C., Z. K., and Y. S. wrote the manuscript with input from all coauthors. Y. S. supervised the research.

Acknowledgment

National Natural Science Foundation of China (62135011&62335001&62575259); the Fundamental Research Funds for the Central Universities.

Data availability

The data that support the plots within this paper and other findings of this study are available from the corresponding authors upon reasonable request.

Code availability

All codes used in this paper are available from the corresponding authors upon reasonable request.

References

1. LiDAR drives forwards (2018) Nat Photonics 12:441–441
2. Guo X et al (2026) Millimeter-Wave Integrated Sensing and Communication System Based on a Photonics-Assisted Phased Array. Laser Photon Rev

3. He J, Yang K, Chen H-H (2021) 6G Cellular Networks and Connected Autonomous Vehicles. IEEE Netw 35:255–261
4. Zhang X, Kwon K, Henriksson J, Luo J, Wu MC (2022) A large-scale microelectromechanical-systems-based silicon photonics LiDAR. Nature 603:253–258
5. Li Y et al (2025) Integrated Optical Wireless Communication Featured With Optical Phased Array Transceivers for Full-Duplex and NonLine-of-Sight Transmission. Laser Photon Rev 20
6. Zhou Z et al (2024) Butler matrix enabled multi-beam optical phased array for two-dimensional beam-steering and ranging. Photonics Res 12:912–920
7. Ma X et al (2026) Multi-target and ultra-high-speed optical wireless communication using a thin-film lithium niobate optical phased array. Nat Commun 17:969
8. Kippenberg TJ, Gaeta AL, Lipson M, Gorodetsky ML (2018) Dissipative Kerr solitons in optical microresonators. Science 361
9. Helgason OB et al (2023) Surpassing the nonlinear conversion efficiency of soliton microcombs. Nat Photonics 17:992–999
10. Ye Z et al (2023) Foundry manufacturing of tight-confinement, dispersion-engineered, ultralow-loss silicon nitride photonic integrated circuits. Photonics Res 11:558–568
11. Chang L, Liu S, Bowers JE (2022) Integrated optical frequency comb technologies. Nat Photonics 16:95–108
12. Marin-Palomo P et al (2017) Microresonator-based solitons for massively parallel coherent optical communications. Nature 546:274–279
13. Jørgensen AA et al (2022) Petabit-per-second data transmission using a chip-scale microcomb ring resonator source. Nat Photonics 16:798–802
14. Feldmann J et al (2021) Parallel convolutional processing using an integrated photonic tensor core. Nature 589:52–58
15. Yu X et al (2025) Parallel optical computing capable of 100-wavelength multiplexing. *eLight* 5
16. Riemensberger J et al (2020) Massively parallel coherent laser ranging using a soliton microcomb. Nature 581:164–170
17. Chen R et al (2023) Breaking the temporal and frequency congestion of LiDAR by parallel chaos. Nat Photonics 17:306–314
18. Lukashchuk A, Riemensberger J, Karpov M, Liu J, Kippenberg TJ (2022) Dual chirped microcomb based parallel ranging at megapixel-line rates. Nat Commun 13:3280
19. Lukashchuk A, Riemensberger J, Tusnin A, Liu J, Kippenberg TJ (2023) Chaotic microcomb-based parallel ranging. Nat Photonics 17:814–821
20. Chen R et al (2025) Integrated bionic LiDAR for adaptive 4D machine vision. Nat Commun 17:24
21. Poulton CV et al (2022) Coherent LiDAR With an 8,192-Element Optical Phased Array and Driving Laser. IEEE J Sel Top Quantum Electron 28:1–8
22. Shekhar S et al (2024) Roadmapping the next generation of silicon photonics. Nat Commun 15:751

23. Kim I et al (2021) Nanophotonics for light detection and ranging technology. Nat Nanotechnol 16:508–524
24. Chen B et al (2024) SiN-On-SOI Optical Phased Array LiDAR for Ultra-Wide Field of View and 4D Sensing. Laser Photon Rev 18:2301360
25. Poulton CV et al (2019) Long-Range LiDAR and Free-Space Data Communication With High-Performance Optical Phased Arrays. IEEE J Sel Top Quantum Electron 25:1–8
26. Chen J et al (2025) Single soliton microcomb combined with optical phased array for parallel FMCW LiDAR. Nat Commun 16:1056
27. Shu H et al (2022) Microcomb-driven silicon photonic systems. Nature 605:457–463
28. Lian D et al (2025) Tunable Optical Orbital Angular Momentum Beams Generation Using 2D Optical Phased Array with an Ultra-Large Reconstructed Envelope. Laser Photon Rev 19
29. Zhao S et al (2024) Low sidelobe silicon optical phased array with Chebyshev amplitude distribution. Nanophotonics 13:263–269
30. Liu Y, Meng X, Hu H (2025) 1000-Channel Integrated Optical Phased Array with 180° Field of View, high resolution and high scalability. Photonics Res 14:1035–1052
31. Miller SA et al (2020) Large-scale optical phased array using a low-power multi-pass silicon photonic platform. Optica 7:3–6
32. Xu W et al (2023) Fully Integrated Solid-State LiDAR Transmitter on a Multi-Layer Silicon-Nitride-on-Silicon Photonic Platform. J Lightwave Technol 41:832–840
33. Hong S et al (2025) Versatile parallel signal processing with a scalable silicon photonic chip. Nat Commun 16:288
34. Liu Y et al (2024) A fully hybrid integrated erbium-based laser. Nat Photonics 18:829–835
35. Xiang C et al (2021) High-performance lasers for fully integrated silicon nitride photonics. Nat Commun 12:6650
36. Sayyah K et al (2022) Fully Integrated FMCW LiDAR Optical Engine on a Single Silicon Chip. J Lightwave Technol 40:2763–2772
37. Mahmudlu H et al (2023) Fully on-chip photonic turnkey quantum source for entangled qubit/qudit state generation. Nat Photonics 17:518–524
38. Rogers C et al (2021) A universal 3D imaging sensor on a silicon photonics platform. Nature 590:256–261
39. Xiang C et al (2021) Laser soliton microcombs heterogeneously integrated on silicon. Science 373:99–103
40. Stern B, Ji X, Okawachi Y, Gaeta AL, Lipson M (2018) Battery-operated integrated frequency comb generator. Nature 562:401–405
41. Sun W et al (2025) A chip-integrated comb-based microwave oscillator. Light Sci Appl 14:179
42. Snigirev V et al (2023) Ultrafast tunable lasers using lithium niobate integrated photonics. Nature 615:411–417

43. Lihachev G et al (2022) Low-noise frequency-agile photonic integrated lasers for coherent ranging. Nat Commun 13:3522
44. Liu C et al (2025) Fast-Tuning and Narrow-Linewidth Hybrid Laser for FMCW Ranging. Laser Photonics Rev 19:2401338
45. Wang S et al (2024) High-Performance Integrated Laser Based on Thin-Film Lithium Niobate Photonics for Coherent Ranging. Laser Photon Rev 18:2400224
46. Liu Y et al (2022) A photonic integrated circuit-based erbium-doped amplifier. Science 376:1309–1313
47. Tran MA et al (2022) Extending the spectrum of fully integrated photonics to submicrometre wavelengths. Nature 610:54–60

Figures

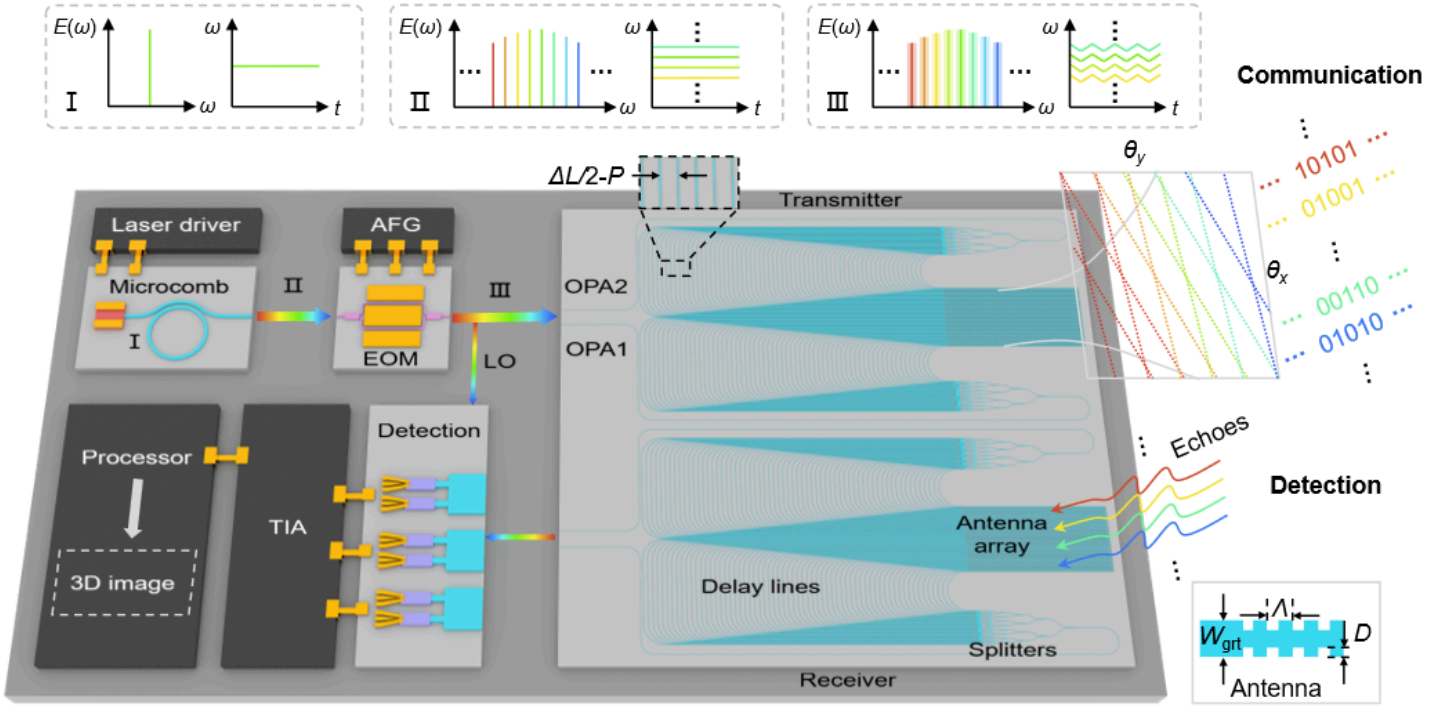


Figure 1

Schematic of the proposed parallel all-solid-state FMCW transceiving LiDAR and FSOC. The comb is generated by pumping a SiN microring resonator with a CW laser, followed by simultaneous modulation of all comb teeth to create linear frequency chirps or individual modulation of each comb tooth to load data stream, and subsequent emission into free space by OPA (Transmitter) to produce distinguishable parallel beams. The echoes of chirp signal are received by another OPA (Receiver), mixed with the local oscillator, and a 3D map could be obtained through processing of the detected signals. AFG, arbitrary

function generator; EOM, electro-optical modulator; LO, local oscillator; OPA, optical phased array; TIA, transimpedance amplifier.

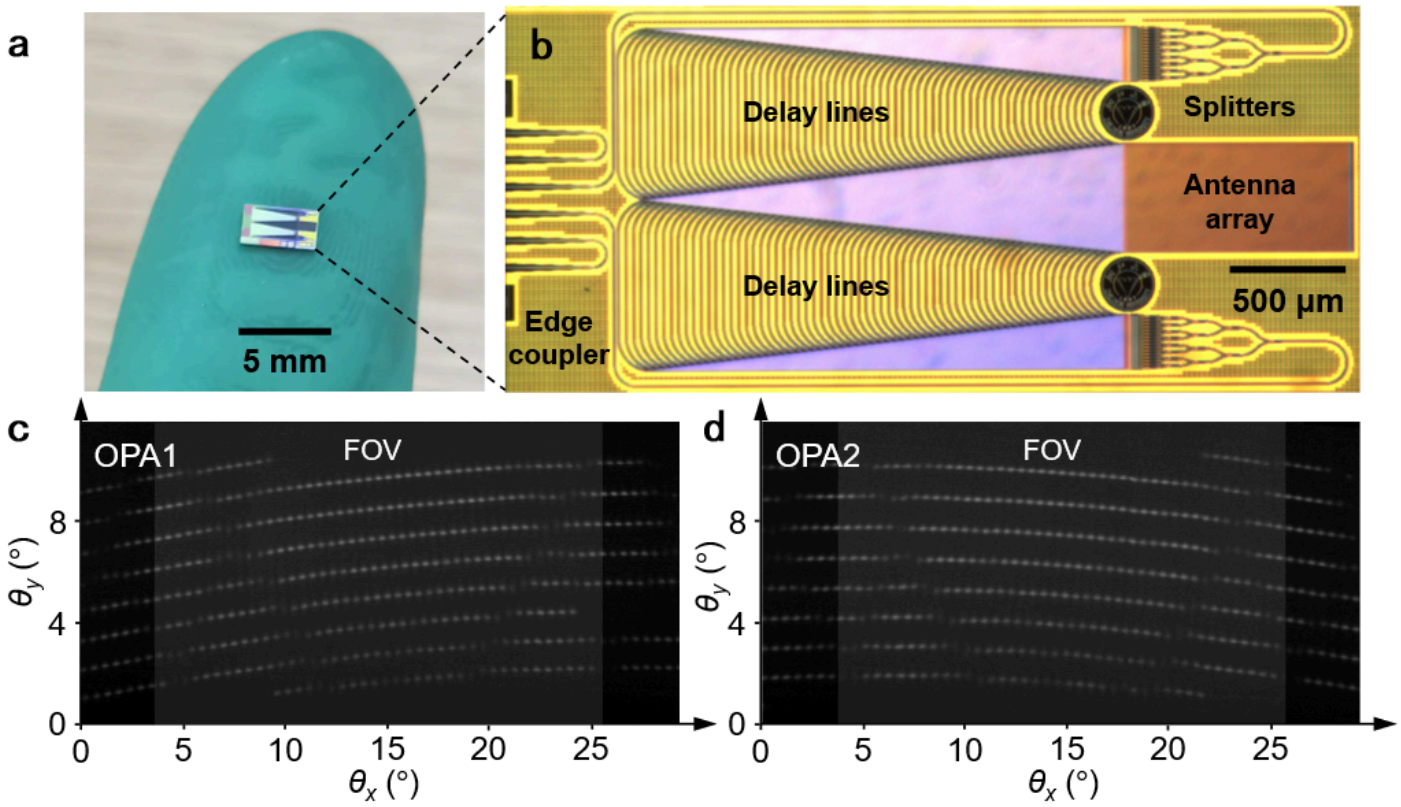


Figure 2

Images and measured far-field beam of the fabricated OPA chip. (a) The picture of the fabricated OPA chip on a fingertip. (b) Optical microscopy image of the fabricated OPA chip. The far-field beam images of (c) OPA1 and (d) OPA2 with wavelength scan from 1510 to 1640 nm at 0.4 nm steps.

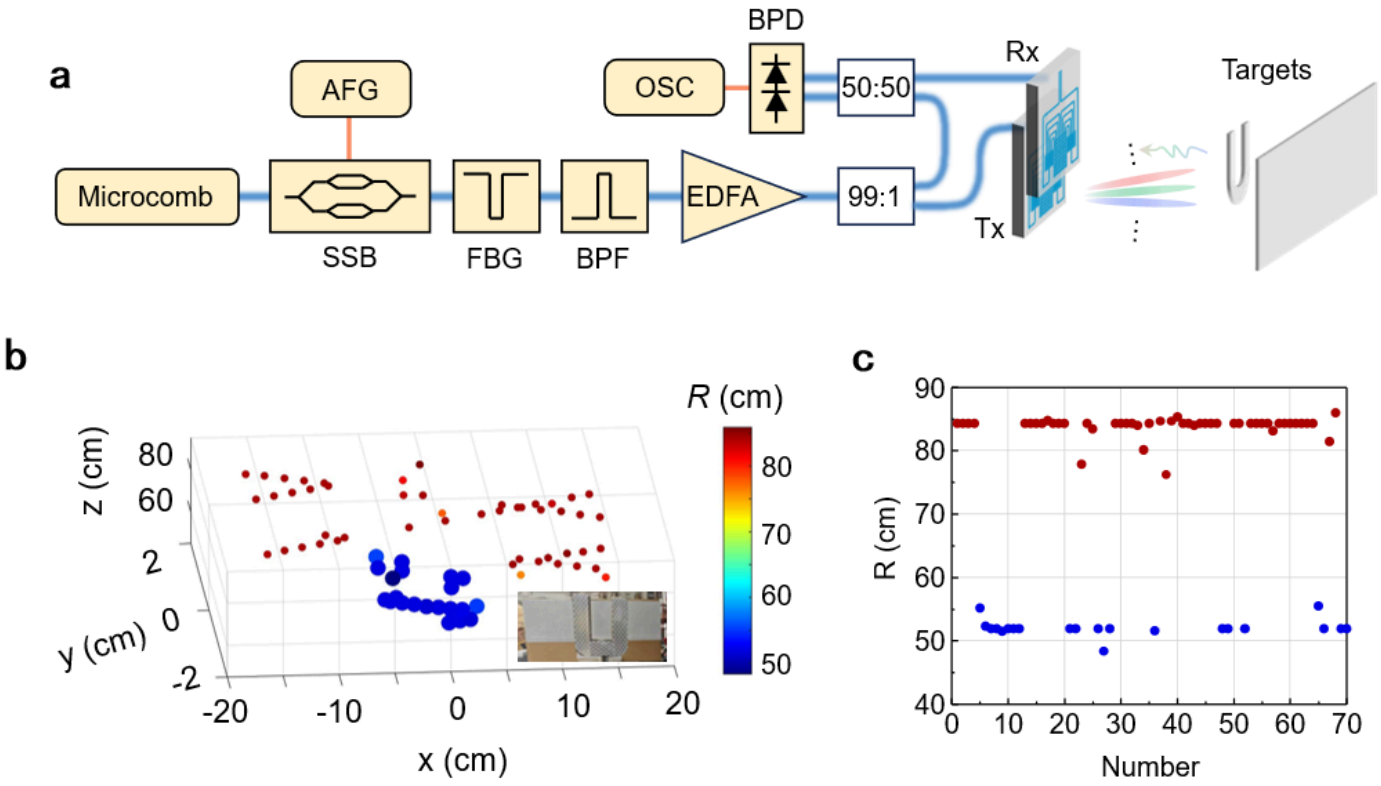


Figure 3

Demonstration of parallel FMCW detection. (a) Schematic of the parallel FMCW LiDAR setup. (b) Measured 3D point clouds and the image of the targets. (c) Measured distances of different beams. SSB, single-sideband modulator; FBG, fiber Bragg grating; BPF, bandpass filter; EDFA, erbium-doped fiber amplifier; BPD, balanced photodetector; OSC, oscilloscope.

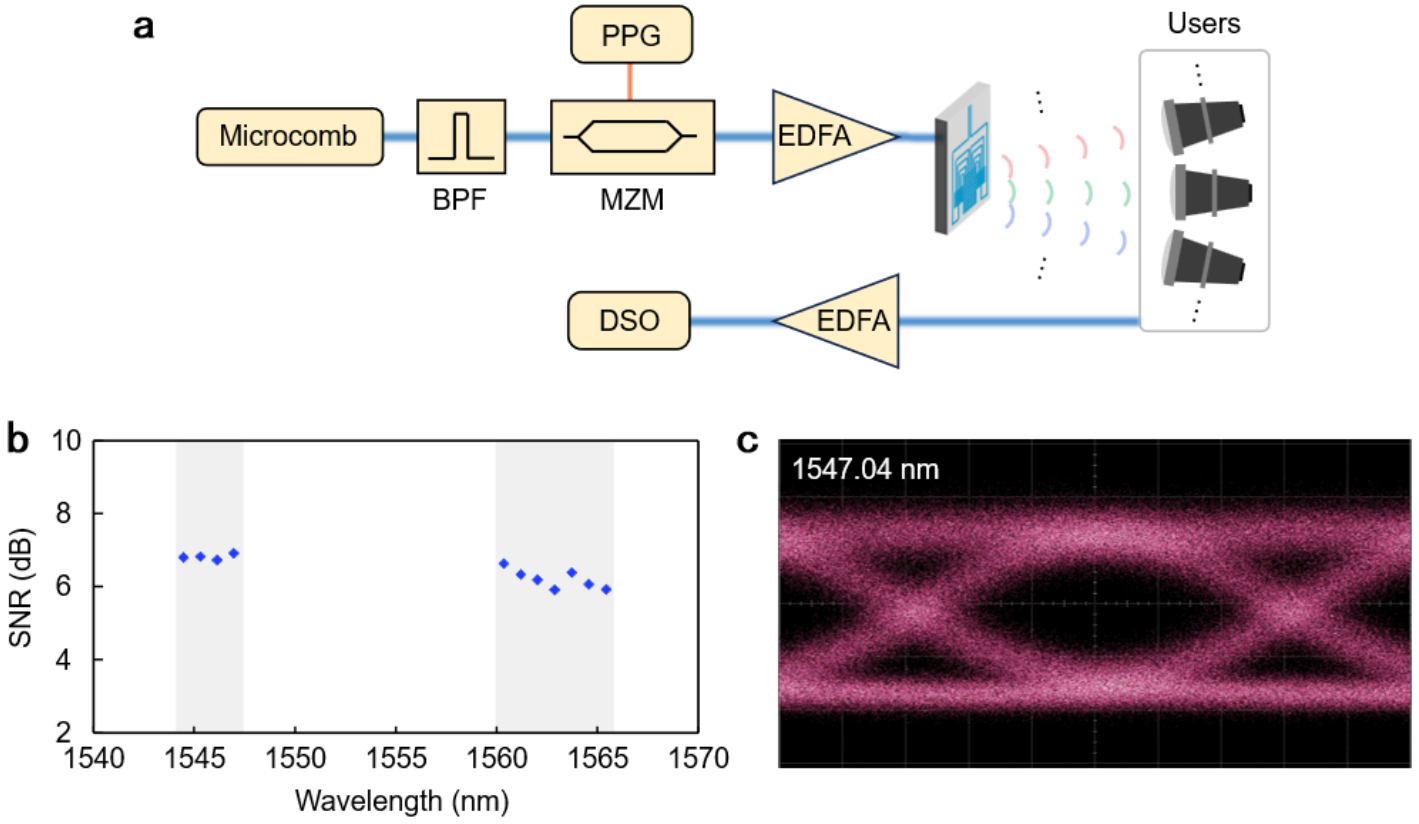


Figure 4

Demonstration of parallel free space communication. (a) Schematic of the parallel free space communication setup. (b) Measured eye mode SNRs of NRZ signals for different comb teeth. (c) Measured eye diagram of NRZ signal for comb tooth with wavelength of 1547.04 nm. MZM, Mach-Zehnder modulator; PPG, programmable pulse generator; DSO, digital sampling oscilloscope.

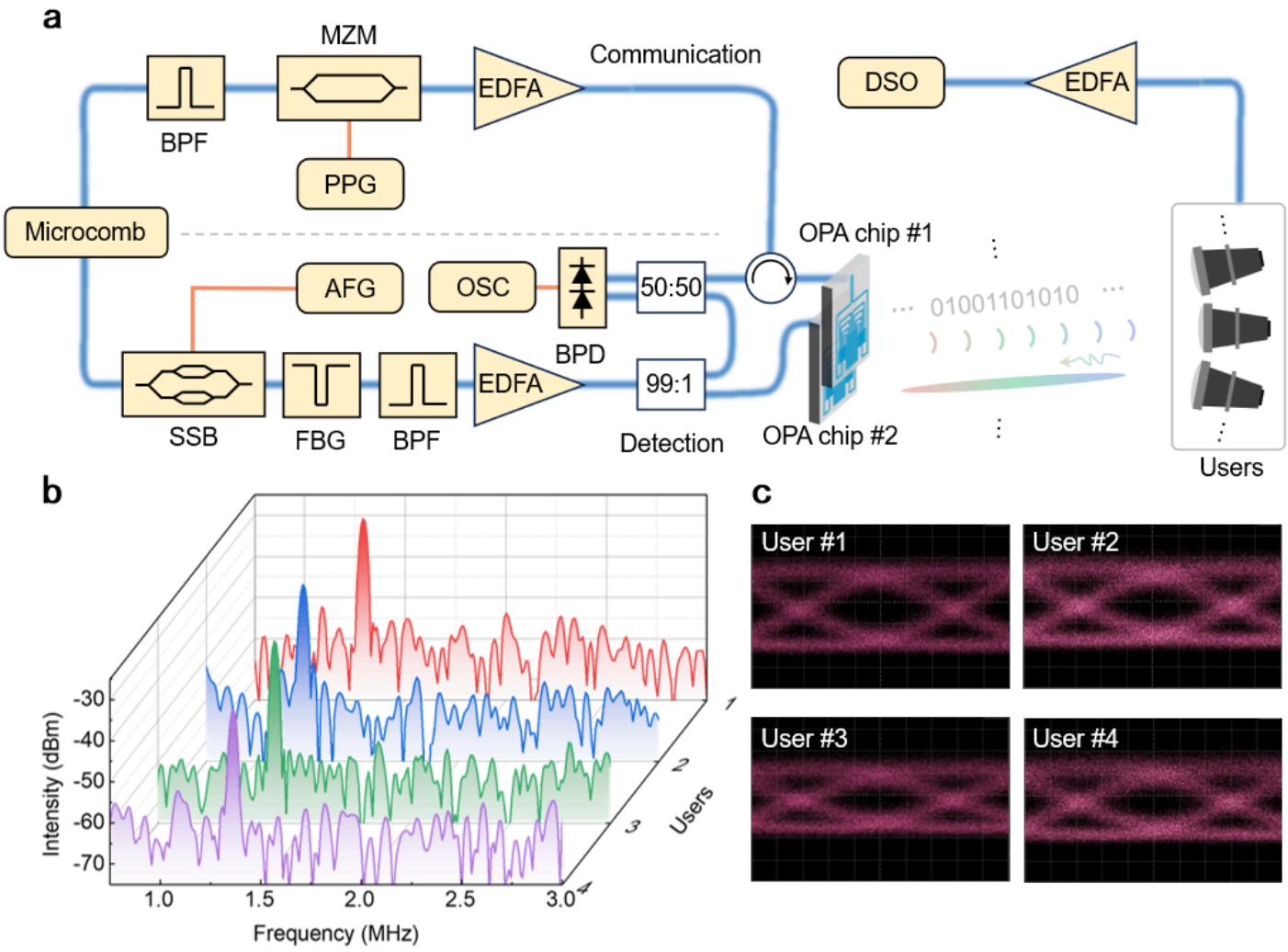


Figure 5

Demonstration of parallel IDC. (a) Schematic of the parallel IDC setup. (b) Beat signal spectra with beam incident on users. (c) Measured eye diagrams of NRZ signals for users.

Supplementary Files

This is a list of supplementary files associated with this preprint. Click to download.

- ParalleldetectioncommunicationSupplementaryForSub.docx